Model tests and numerical simulations on shallow circular tunneling

Nagoya Institute of Technology, Researcher	Member	H. M. Shahin
Nagoya Institute of Technology, Professor	Member	Teruo Nakai, Feng Zhang
Nagoya Institute of Technology, Researcher	Member	Mamoru Kikumoto
Nagoya Institute of Technology, Graduate Student	Student Member	Yusuke Tabata, Eriko Nakahara

ABSTRACT

In our previous researches, we carried out model tests on tunnel excavation using trap-door tunnel apparatus to investigate the deformation mechanism and redistribution of stress surrounding the tunnel. Recently, we have developed a new and more realistic tunnel apparatus where the cross section of the tunnel is circular. The apparatus can simulate various excavation methods such as full face excavation, top and side drift and bench cut excavation. In this present research, two-dimensional model tests on tunnel excavation using the newly developed circular tunnel apparatus are performed. Numerical simulations are also conducted using finite element method considering plane strain drained condition. In the finite element analyses elasto-plastic subloading t_{ij} model is used as a constitutive model of the ground material. It is revealed in this research that volume loss is less significant compare to the crown drift in the case of shallow tunneling. The numerical results show very good agreement with the results of the model tests.

1. INTRODUCTION

Shallow tunneling is one of the essential methods to make underground space in congested urban areas. With the ongoing demand of tunneling technology research works on ground movements and earth pressures due to tunnel excavation have been potentially increased. The trap door apparatus has been used to investigate the mechanism of tunneling problems by many researchers (Murayama and Matsuoka, 1971; Adachi et al. 1994, Nakai et al., 1997; Shahin et al., 2004). In our previous work, we have been carried out laboratory model tests using trap-door tunnel apparatus to investigate the deformation mechanism and redistribution of stress at the level of tunnel elevation. However, with the trap door apparatus the earth pressures around the tunnel can not be measured except the tunnel crown. Considering this point a new and more realistic tunnel apparatus has been developed where the cross section of the tunnel is circular. With the new apparatus earth pressure can be measured around the tunnel periphery. The apparatus can simulate various excavation methods such as full face excavation, top and side drift and bench cut excavation.

This paper explains the 2D model tests on tunnel excavation with the newly developed circular tunnel apparatus and numerical analyses using the subloading t_{ij} model. This model can consider influence of intermediate principal stress on the deformation and strength of soils, Dependence of the direction of plastic flow on the stress paths, Influence of density and/or confining pressure on the deformation and strength of soils. In this paper, the deformation mechanism is described focusing the ground movements and shear strain patterns. The movements and distributions of shearing strain in the ground are measured using Particle Image Velocimetry technique.

2. DESCRIPTION OF MODEL TESTS

Apparatus of the model test

Figure 1 shows a schematic diameter of 2D tunnel apparatus. Figure 2 represents a newly developed model tunnel with circular cross section. It consists of a shim at the center of the tunnel surrounded with 12 segments. The segments are strongly tightened all around the shim with rubber band. One motor is attached with the shim to pull it out in the horizontal direction. The model tunnel is kept in space with a vertical shaft, and can be moved in the vertical direction with another motor. Therefore, the device consists of two motors - one is for shrinking the tunnel and the other for moving the tunnel vertically to fix it at a chosen ground depth. It is possible to make these motors work simultaneously and individually together with controlling the speed of the motors. With the motor the shim is pulled out gradually which changes the diameter of the shim, consequently the segments move inward direction towards the center of the tunnel and the diameter of the tunnel is reduced. Changing the shape of the shim different kinds of excavation process, such as full face excavation, top and side drift and bench cut excavation can be reproduced with this apparatus. The reduction of tunnel diameter and the amount of radial shrinkage are obtained from a dial gauge reading which is determined from the calibration result. The vertical movement (if requires to impose) of the tunnel is also measured with another dial gauge. Therefore, the shrinkage of the tunnel can be attained in a controlled manner, which can simulate the condition of a real tunnel construction.

In the apparatus 12 load cells are used to measure earth pressure acting on the tunnel. The load cells are attached with the block which is placed surrounding the segments of the tunnel. Each load cell block is 2.35cm in width and 5.0cm in length. The blocks are tightly fastened with some rubber bands. Therefore, earth pressure can

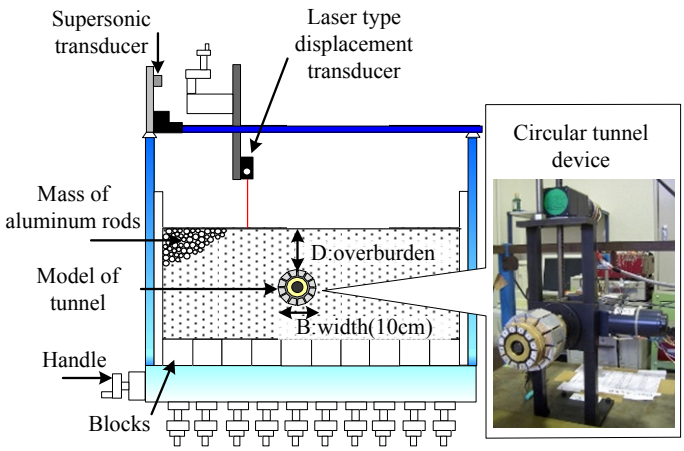

Fig. 1: Schematic diagram of 2D tunnel apparatus

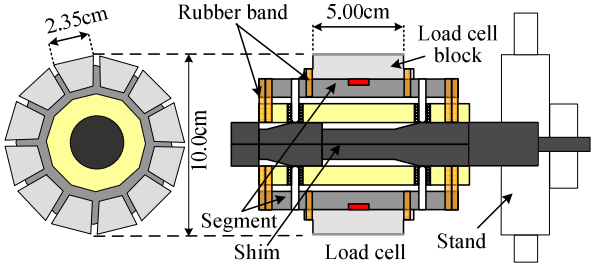

Fig. 2: Circular tunnel device

be obtained at 12 points on the periphery of the tunnel at a time. Earth pressure can also be obtained at other positions by rotating the tunnel. However, in this case it will be required to make the ground again. Including the load cell bocks the diameter of the model tunnel is 10.0cm. The circular tunnel device is placed on an iron table that was used for the trap door tunnel apparatus (Nakai et al., 1997; Shahin et al., 2004). It has 10 moveable blocks above which the ground is made. The reason of using this type of base is to adjust the initial stress condition of the ground such as the stress distribution becomes similar to the ground where no tunnel is set up. The surface settlement of the ground is measured using a laser type displacement transducer with an accuracy of 0.01mm and its position in the horizontal direction is incurred with a supersonic wave transducer. Photographs are taken during experiments which are later on used as input data for the simulation of ground movements with Particle Image Velocimetry.

Preparation of Model Ground and Excavation Patterns

Firstly, the tunnel device is set at a height of 10cm; the height is measured from the bottom boundary to the tunnel invert. Varying the distance between the tunnel invert and the bottom boundary, several experiments were conducted. It was found that this height (10cm) is free from the influence of the bottom boundary. After setting the tunnel device, mass of aluminum rods, having diameters of 1.6 and 3.0mm and mixed in a ratio of 3:2 in weight, is stacked up to a prescribed depth. The unit weight of the aluminum rod mass is 20.4kN/m^3, and the length is 5.0cm. The initial ground is made is such a way so that the earth pressure becomes similar to the earth pressure at rest adjusting the bottom moveable blocks of the apparatus. Great care is taken to make a uniform ground and not to apply any undesired load in the ground.

In this study two types of excavation patterns are considered. Pattern 1 (full face excavation) corresponds to the excavation where the center of the tunnel is kept fixed and the diameter of the tunnel is reduced applying shrinkage of 4mm all around the tunnel as shown in Figure 3. Pattern 2 represents the excavation pattern where the invert is kept fixed (top drift excavation). This is obtained by descending the tunnel during the application of shrinkage. Here, the same amount of shrinkage (4mm) is applied. However, as the center is moved downward by 4mm the amount of imposed displacement at the tunnel crown is 8mm. In the both excavation patterns the volume loss of the ground is the same, which is equal to 15.36%. The data at different volume losses started from 0.20% are recorded in the experiments. The model tests have been conducted for four kinds of overburden ratio, *D/B* equals 0.5, 1.0, 2.0 and 3.0, where *D* is the depth from the ground surface to the top of the tunnel and *B* (10cm) is the width of the tunnel. In Figure 3, d_r represents the amount of shrinkage towards the center of the tunnel, and d_c indicates the amount of displacement at the tunnel center.

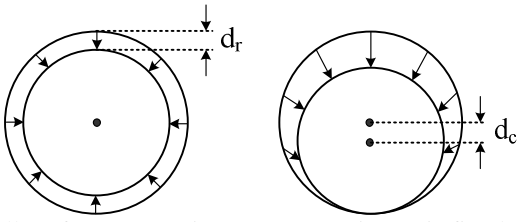

(I) center is fixed (full surface excavation) (II) invert is fixed (top drift excavation)

Fig. 3: Excavation patterns

3. NUMERICAL ANALYSIS

Figure 4 shows the mesh, for the case of *D/B*=2.0, used in the finite element analyses. Isoparametric 4-noded elements are used in the mesh. Smooth boundary conditions are used in the analyses considering both vertical sides of the mesh are free in the vertical direction, and the bottom face is fixed. To simulate the tunnel excavation, vertical displacement is applied up to 4mm to all the nodes at the periphery of the tunnel block for the full face excavation, and for top drift excavation the magnitude of the applied displacement varies from 8mm at the crown node to zero at the invert node. Analyses are carried out with the same scale and same conditions of the model tests considering plane strain drained condition. The small strain theory is used in the numerical simulation. Two-dimensional finite element anlyses are carried out with FEMtij-2D. The stiffness matrix for the ground material is evaluated using Gauss Integration 2 x 2. The constitutive law used in this numerical analysis is the subloading t_{ij} model (Nakai and Hinokio, 2004). Model parameters for the aluminum rod mass are shown in Table 1. The parameters are fundamentally the same as those of the Cam clay model except the parameter *a,* which is responsible for the influence of density and confining pressure. The parameter β represents the shape of yield surface. The parameters can easily be obtained from the traditional laboratory tests. Figure 5 shows the results of the biaxial tests for the mass of aluminum rods used in the model tests. The figure indicates both the positive and negative dilatancy of aluminum rod mass; and it is clear that the strength and deformation behavior is very close to those of dense sand. The dotted lines represent the numerical results for a confining pressure of 1/100 times the confining pressure of experiments. From the stress-strain behavior of the element tests simulated with subloading t_{ij} model, it is noticed that this model can express the dependency of stiffness, strength and dilatancy on the density as well as on the confining pressure. The initial stresses, correspondent to the geostatic (self-weight) condition, are assigned to the ground in all numerical analyses.

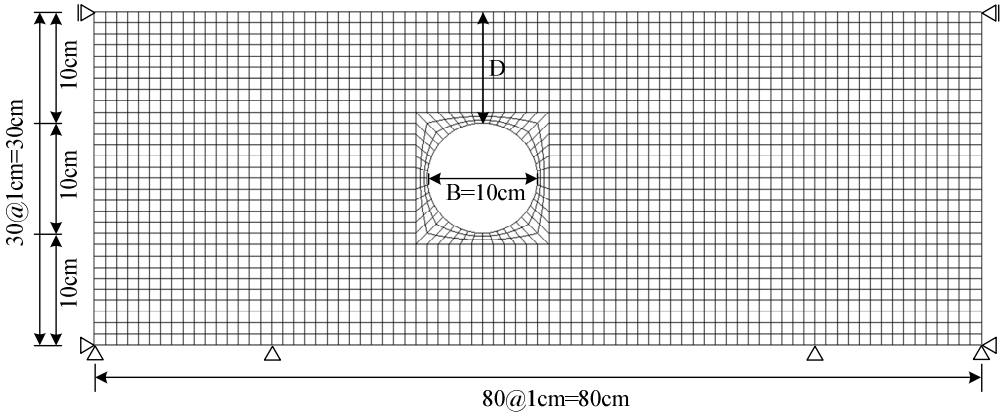

Fig. 4: Finite element mesh (D/B=2.0)

Table 1. Parameters of soil materials

λ	κ	N (e_{NC} *at p=98kPa &=0kPa*)	$R_{CS}=(\sigma_1/\sigma_3)_{CS(comp.)}$	β	ν_e	a
0.008	0.004	0.30	1.80	1.20	0.20	1300

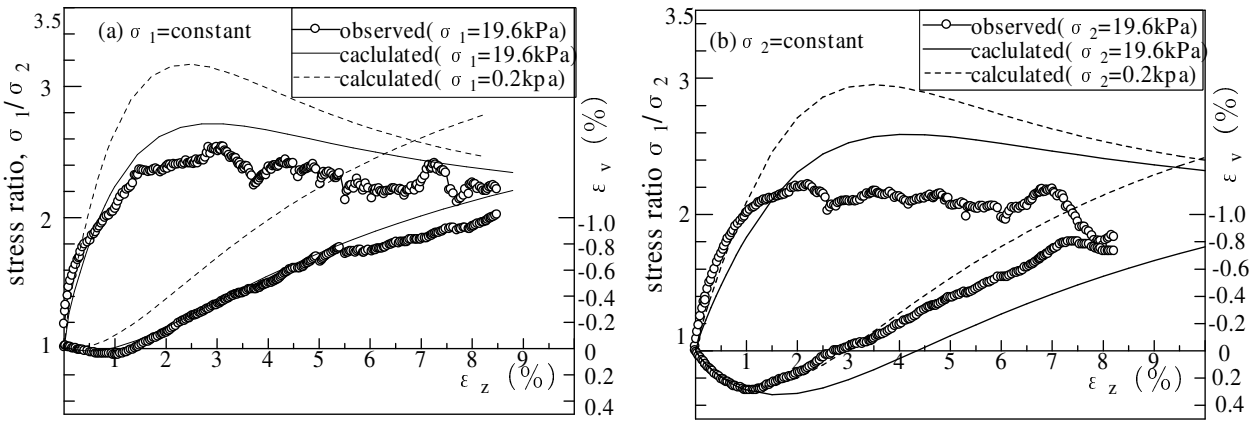

Fig. 5: Stress-strain-dilatancy relation of the mass of aluminum rods

4. RESULT AND DISCUSSION

4.1 Surface settlement

Figure 6 shows the surface settlements troughs of the full surface excavation for the amount of shrinkage d_r=1mm (volume loss = 3.96%) and 4mm (volume loss = 15.36%) in the case of *D/B*=1.0, 2.0 and 3.0. Figure 6a represents the observed results and Figure 6b shows the computed one. Figure 7 represents the same for the top drift excavation. The abscissa represents distance from the center of the tunnel, while the vertical axis shows the amount of surface settlement. For both patterns of excavation the maximum surface settlement occurs vertically above the tunnel crown. Surface settlements become smaller with the increase of the tunnel depth, but they extend over a wider region similar to the previous research conducted with trap door tunnel apparatus (Shahin et al., 2004). The shape of the surface settlement profiles is the same for all the soil covers in the case of full face excavation. For the same volume loss the maximum surface settlement is larger in the case where the invert is fixed than that of the full face excavation. This is because the applied displacement at the crown is 8mm for the fixed invert and 4mm for the full face excavation though the volume loss is the same. Surface settlement occurs

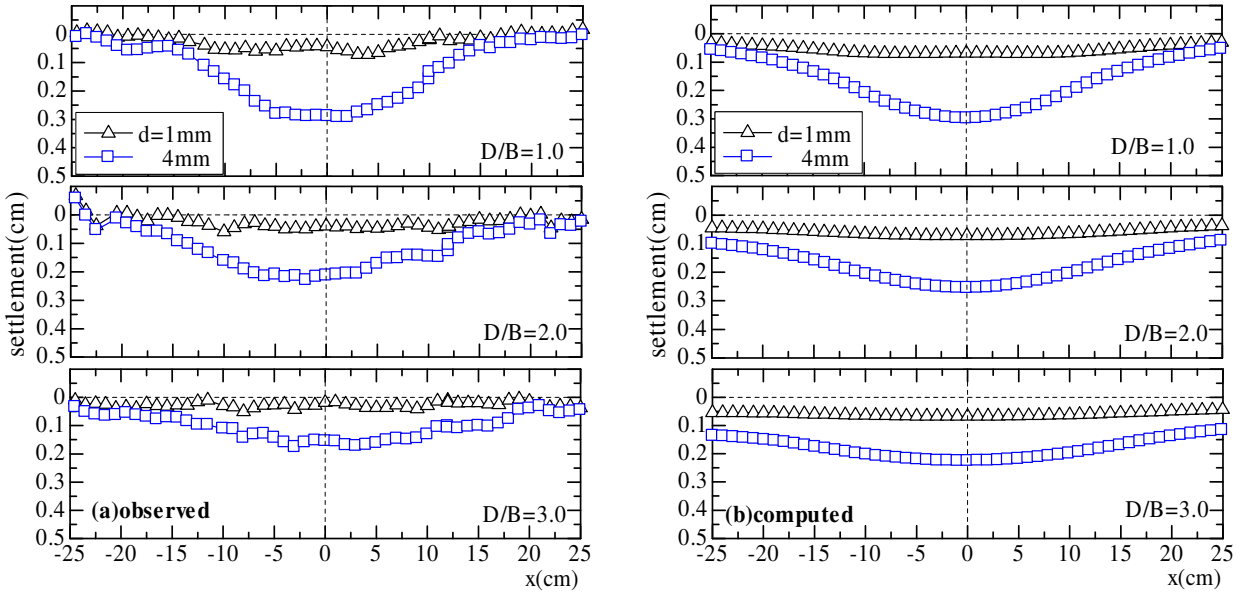

(a) Observed (b) Computed

Fig. 6: Surface settlement profiles: center is fixed

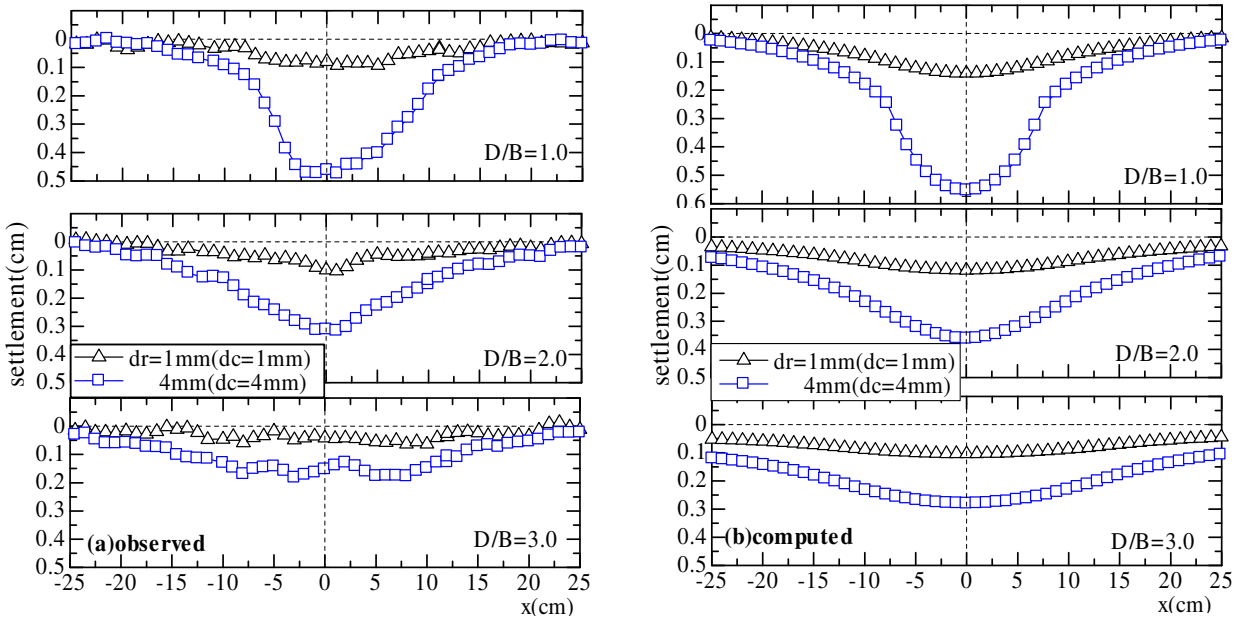

(a) Observed (b) Computed

Fig. 7: Surface settlement profiles: invert is fixed

locally for the 8mm applied displacement in the case of fixed invert, consequently the shape of surface settlement profile varies with the soil cover in this case. The tendency of larger surface settlement for the fixed invert is more significant up to *D/B*=2.0. However, in the case of *D/B*=3.0 the difference of the surface settlement profiles between the two excavation patterns is less significant. From these results it is revealed that for the same volume loss surface settlement profiles vary with the excavation patterns in the case of shallower tunneling. Therefore, the surface settlement may not be properly estimated using the method of volume loss (Mair et al., 1993) for shallow tunneling. The results of numerical analyses show the same tendency of model tests not only in shape but also in quantity.

4.2 Ground Movements and Shear Strains

Figure 8 and 9 represent the observed ground movements and computed displacement vectors for the soil cover D/B=1.0 and 2.0 in case of full face excavation and fixed invert excavation, respectively. Two photos are superimposed in a figure, the first one was taken after initial ground is made and before tunnel excavation, and the other was after squeezing the tunnel by d_r=4mm. The difference between the two photos is darkened using image processing software. The deformed area is bounded with white curves to visualize the range of deformed area in the ground easily in the figures. In the simulations the displacement vectors are taken and their directions represent the direction of ground movements. The magnitude of the displacement vectors is shown with the brightness of the color. It is seen in Figure 8 for the full face excavation the deformation of the ground extends diagonally upward from the tunnel invert. The deformed region becomes wider with deeper grounds as the distance from the surface to the tunnel increases. In the deeper soil covers ground is relatively less distorted near the surface compared to the vicinity of the tunnel. In Figure 9 for the excavation pattern of fixed tunnel invert it is found that the onset of the deformation of the ground is not just from the tunnel invert rather a certain height from it. In this case the range of the deformed region is narrower compare to the full face excavation. The numerical analyses perfectly capture the shapes of the observed deformation zones for different ground depths.

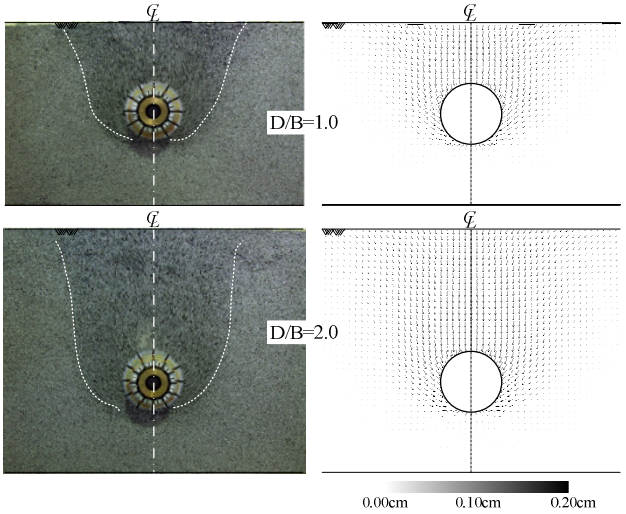

(a) Observed (b) Computed

Fig. 8: Ground movements: center is fixed

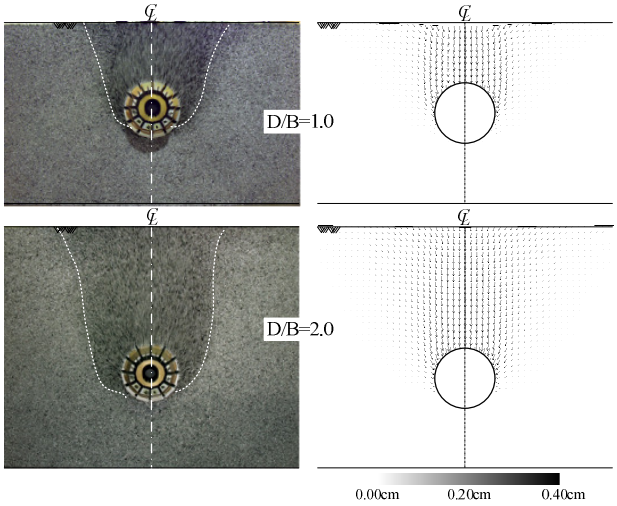

(a) Observed (b) Computed

Fig. 9: Ground movements: invert is fixed

The distribution of shear strain of the model tests are obtained from the simulation of Particle Image Velocimetry (PIV) technique. The PIV is originally developed in the field of fluid mechanics (Adrain, 1991). In this paper, two images are divided into a finite area; the average movement rate of the aluminum rods of each area is being output as nodal displacement. The strain for one grid is calculated from these displacements by using the shape function and the Jacobian matrix that are used in finite element method for displacement and strain relationship. Equation (1) represents the relation between the nodal displacements (*u, v*) and strains of a finite area.

$$\begin{pmatrix} \varepsilon_{xx} \\ \varepsilon_{yy} \\ \gamma_{xy} \end{pmatrix} = \begin{pmatrix} \frac{\partial N_1}{\partial x} & 0 & \frac{\partial N_2}{\partial x} & 0 & \frac{\partial N_3}{\partial x} & 0 & \frac{\partial N_4}{\partial x} & 0 \\ 0 & \frac{\partial N_1}{\partial y} & 0 & \frac{\partial N_2}{\partial y} & 0 & \frac{\partial N_3}{\partial y} & 0 & \frac{\partial N_4}{\partial y} \\ \frac{\partial N_1}{\partial y} & \frac{\partial N_1}{\partial x} & \frac{\partial N_2}{\partial y} & \frac{\partial N_2}{\partial x} & \frac{\partial N_3}{\partial y} & \frac{\partial N_3}{\partial x} & \frac{\partial N_4}{\partial y} & \frac{\partial N_4}{\partial x} \end{pmatrix} \begin{pmatrix} u_1 \\ v_1 \\ u_2 \\ v_2 \\ u_3 \\ v_3 \\ u_4 \\ v_4 \end{pmatrix} \quad (1)$$

where, N is the shape function and can be expressed in terms of the local coordinate system as-

$$N_i = \frac{1}{4}(1+\xi_i\xi)(1+\eta_i\eta) \qquad (2)$$

Figures 10 and 11 show the distribution of shear strain for full face excavation and fixed invert excavation, respectively, in the case of *D/B*=1.0 and 2.0. It is seen in Figure 10 that the shear band of the ground is developed from the tunnel invert and covered the entire tunnel during tunnel excavation for the full surface excavation. For this case shear strain spreads to a wider region similar to the ground movements (Fig.8). From Figure 11 it is seen that shear band develops from the side of the tunnel not from the tunnel invert. In this case the length of the shear band is longer than that of the full face excavation. The different patterns of shearing strain due to the different types of the tunnel excavation lead the change of the ground behavior. The two different excavation patterns produce different kinds of shear strain though the volume loss is the same. The shear strain of the numerical analyses shows very good agreement with the results of the model tests.

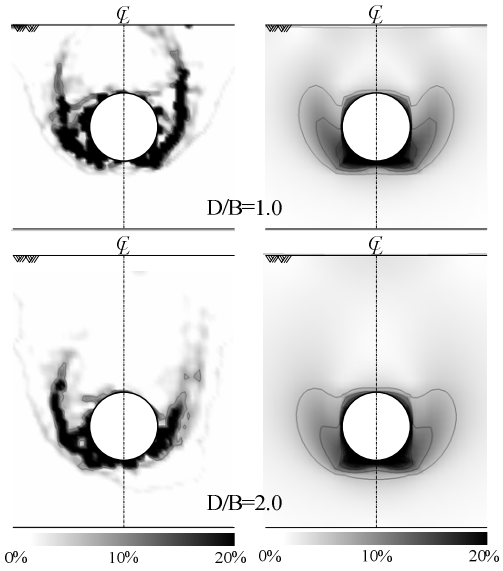

(a) Observed (b) Computed

Fig. 10: Distribution of shear strain: center is fixed

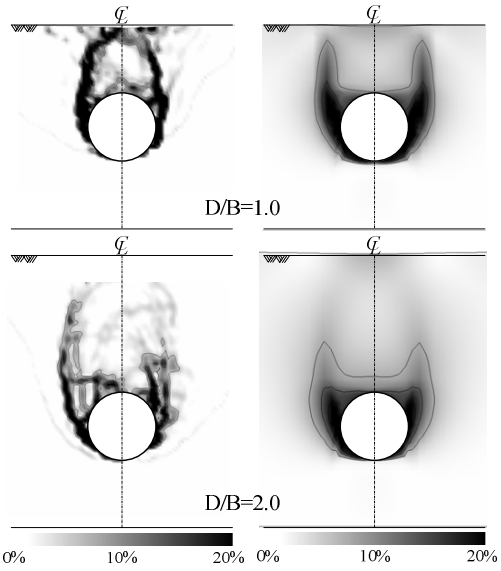

(a) Observed (b) Computed

Fig. 11: Distribution of shear strain: invert is fixed

4.3 Earth pressure

Figure 12 and 13 show the observed and computed earth pressure distributions for *D/B*=1.0 and 2.0 in case of full face excavation and fixed invert excavation, respectively. The plots are drawn in the 12 axes corresponding to the radial direction of the 12 load cells towards the center of the model tunnel. The figures represent the value of earth pressure in Pascal corresponding to the amount of applied displacement (amount of shrinkage). It is seen in Figure 12 that earth pressure decreases all around the tunnel for the full face excavation due to the arching effect. The results appear to be in agreement with the results of tunnel experiments performed by Murayama and Matsuoka, 1971; Adachi et al., 1994; Shahin et al. 2004. As shear band develops surrounding the entire tunnel (Fig.10) the surrounding ground undergoes to loosen state which reduces stresses in that place. It is also noticed that the earth pressure decreases suddenly after applying shrinkage of the tunnel within 0.00 to 0.20mm. Further shrinking the tunnel, earth pressure decreases gradually at a lower rate up to a certain extent after which the earth pressure becomes almost constant. Sudden change in earth pressure is due to soil arching, immediately after disturbing the ground. For the fixed invert excavation earth pressure distributions are different from the full surface excavation. In this case earth pressure decreases all around the tunnel till d_r=1mm, for further shrinkage of the tunnel it increases in the bottom part of the tunnel while it remains almost same in the upper part of tunnel. It can be explained with the shear strain distribution shown in Figure 11. As the ground becomes loosen only in the upper part of the tunnel after d_r=1mm, the confining pressure in the bottom part increases, therefore, the increase of earth pressure in the bottom part of tunnel can be speculated. From the above discussions it can be said that the distribution of earth pressure is highly dependent on the excavation patterns.

Figure 14 and 15 illustrates the change of earth pressure at load cells 4 and 9 against the amount of shrinkage for different soil covers. Load cell 4 is located in the vicinity of the tunnel crown, and load cell 9 is in the vicinity of the tunnel invert. This figure confirms the sharp change of earth pressure during tunnel excavation. In the case of fixed invert excavation (Fig.15), at the position of load cell 9 earth pressures increases after around d_r=1mm, which is different from the results of the full face excavation (Fig.14) where earth pressure remain

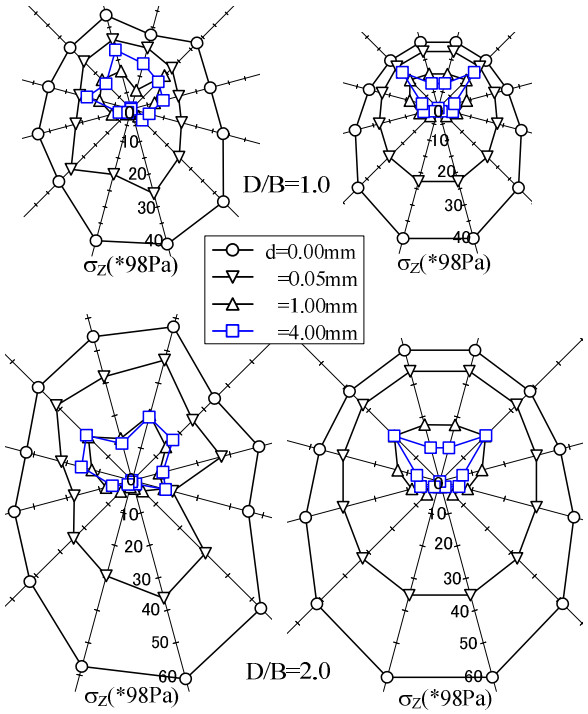

(a) Observed (b) Computed

Fig. 12: Distribution of earth pressure: center is fixed

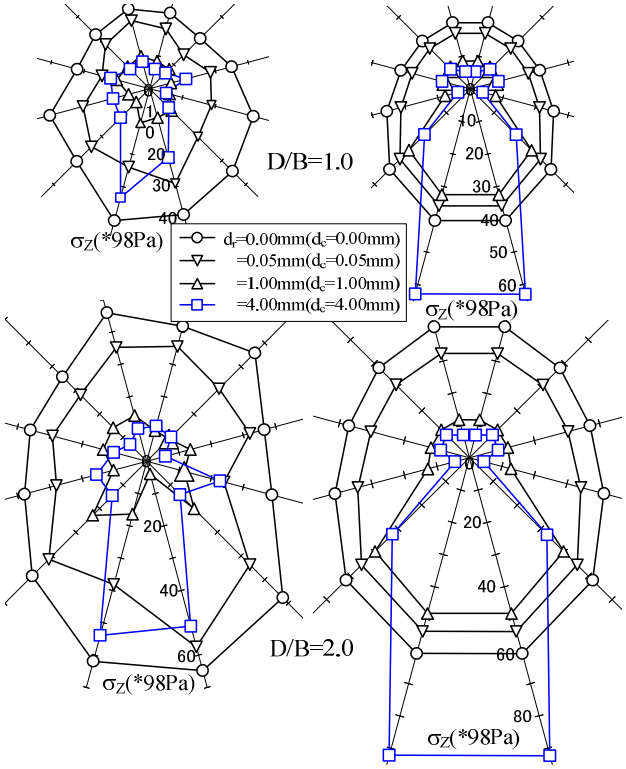

(a) Observed (b) Computed

Fig. 13: Distribution of earth pressure: invert is fixed

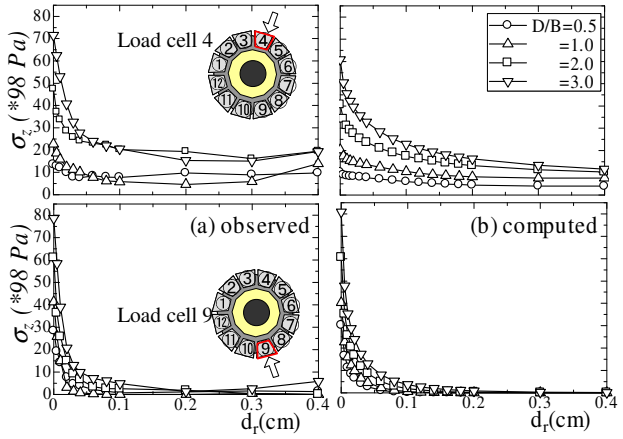

(a) Observed (b) Computed

Fig. 14: Earth pressure history: center is fixed

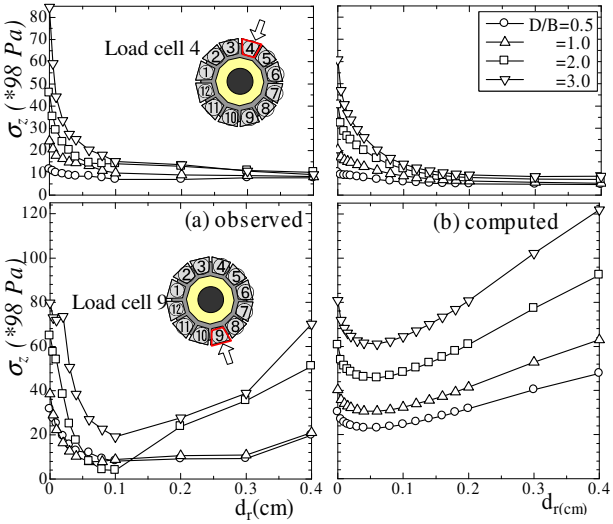

(a) Observed (b) Computed

Fig. 15: Earth pressure history: invert is fixed

constant after that amount of shrinkage. The phenomenon of the earth pressure increase after reduction to some extent can be described as the change of arching effect due to the non-linear and elastoplastic behavior of the ground materials. It can not be described with a usual linear elastic model. The results of numerical analyses are in good agreement with the results of model tests. Therefore, it can be said that a proper elastoplastic constitutive model is required to predict earth pressure around tunnel for lining design.

5. COMPARISONS WITH ELASTIC ANALYSIS

In this study numerical analyses with a linear elastic theory are carried out to compare the results with the elastoplastic analyses. This section describes some typical results of the analyses. Young's modulus for elastic analyses is calculated from the stress-strain relation (Fig.16) of biaxial test performed in laboratory for the mass of aluminum rods. The value of E=5500kPa is chosen from the figure, and the assumed value of Poisson's ratio is 0.33 for the ground of aluminum rods mass.

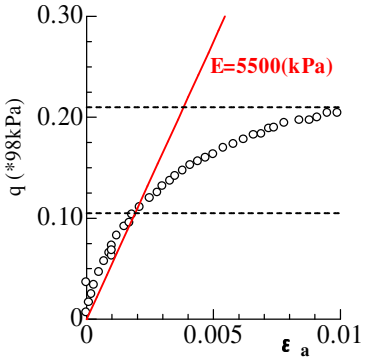

Fig. 16: Stress-strain relation of aluminum rods mass

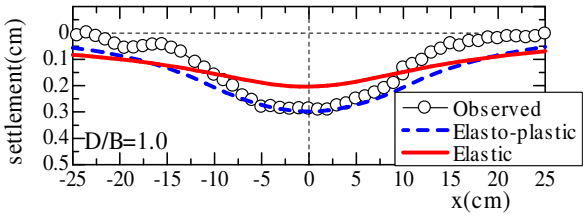

Fig. 17: Comparisons of surface settlement profiles

Figure 17 shows the surface settlement profiles of the model test, elastoplastic analysis and elastic analysis for soil cover *D/B*=1.0. It is seen in this figure that elastoplastic analysis can precisely express the results of the model test. The elastic analysis produces a wider surface settlement profiles compare to the observed one, the maximum surface settlement is smaller as well. As there is no yield point in a liner elastic model it can not express the deformation occurred locally. In this analysis displacement is applied to simulate tunnel excavation, therefore, there is no relation of the magnitude of the Young's modulus in the shape of the settlement trough except the Poisson's ratio.

CONCLUSION

To investigate the deformation mechanism and earth pressure of the ground, a new and more realistic tunnel apparatus has been developed. With this apparatus 2D model test and elastoplastic finite element analyses are carried out. From the model tests and numerical analyses, the following points can be concluded:

(1) Surface settlement and earth pressure around tunnel are significantly influenced by the displacement applied at the tunnel crown for the same overburden and the same volume loss.

(2) The volume loss is less significant compare to the crown drift in the case of shallow tunneling.

(3) Full face excavation produces wider range of the deformed region compare to the top drift (fixed invert) excavation.

(4) The ground deformation mechanisms are different for the same volume loss with different excavation patterns. Excavation patterns control the deformation mechanism of the ground during tunnel excavation.

(5) The distribution of earth pressure is highly dependent on the excavation patterns. If the excavation patterns during tunnel excavation are different, these will produce different magnitude of earth pressure even though the volume losses are the same.

The finite element analysis with subloading t_{ij} model is a powerful tool to predict earth pressure and ground behavior during tunnel excavation

REFERENCE

1) Adachi, T., Tamura, T., Kimura, M. & Aramaki, S. 1994. Earth pressure distribution in trap door tests: *Proc. of 29th Japan National Conference of SMFE*, 3, 1989-1992.
2) Adrain, R. J. 1991. Particle imaging techniques for experimental fluid mechanics: *Ann. Rev. Fluid Mech.* 23, 261-304.
3) Murayama, S. and Matsuoka, H. 1971. Earth pressure on tunnels in sandy ground: *Proc. of JSCE*, 187: 95-108 (in Japanese.
4) Mair, R.J., Taylor, R.N. & Bracegirdle, A. 1993. Subsurface settlement profiles above tunnels in clays. Geotechnique 43, No.2, 315-320.
5) Nakai, T., Xu, L. & Yamazaki, H. (1997): 3D and 2D model tests and numerical analyses of settlements and earth pressure due to tunnel excavation, *Soils and Foundations*, 37(3), 31-42.
6) Nakai, T., and Hinokio, M. 2004. A simple elastoplastic model for normally and over consolidated soils with unified material parameters. *Soils and Foundation.* 44(2): 53-70.
7) Shahin, H. M., Nakai, T., Hinokio, M., Kurimoto, T., and Sada, T. (2004): Influence of surface loads and construction sequence on ground response due to tunneling, *Soils and Foundation*, 44(2), 71-84.